JCB Journal of Cell Biology

REPORT

Loss of centromeric RNA activates the spindle assembly checkpoint in mammalian female meiosis I

Tianyu Wu[1], Simon I.R. Lane[2], Stephanie L. Morgan[3], Feng Tang[4], and Keith T. Jones[5]

The repetitive sequences of DNA centromeric regions form the structural basis for kinetochore assembly. Recently they were found to be transcriptionally active in mitosis, with their RNAs providing noncoding functions. Here we explore the role, in mouse oocytes, of transcripts generated from within the minor satellite repeats. Depletion of minor satellite transcripts delayed progression through meiosis I by activation of the spindle assembly checkpoint. Arrested oocytes had poorly congressed chromosomes, and centromeres were frequently split by microtubules. Thus, we have demonstrated that the centromeric RNA plays a specific role in female meiosis I compared with mitosis and is required for maintaining the structural integrity of centromeres. This may contribute to the high aneuploidy rates observed in female meiosis.

Introduction

During chromosome segregation, the kinetochore forms the mechanical basis of chromosome attachment to the spindle, facilitating correct orientation and movement at anaphase. The kinetochore also acts as the signaling hub for the spindle assembly checkpoint (SAC), which ensures that chromosome segregation occurs only after correct attachment of all kinetochores (Musacchio and Salmon, 2007; Jones and Lane, 2013). The kinetochore is therefore essential in preventing aneuploidy.

In most organisms, the kinetochore is built on repetitive DNA sequences (centromeric DNA; Fukagawa and Earnshaw, 2014), a region of heterochromatin denoted epigenetically and loaded with CENPA (centromeric protein A) containing nucleosomes (Gent and Dawe, 2012; Earnshaw, 2015). For example, in the mouse, this region is comprised of highly ordered 123-bp repeats, termed minor satellite (MinSAT) repeats (Bouzinba-Segard et al., 2006; Ideue and Tani, 2020). Such repeats contain a concentration of CENPA nucleosomes, providing a direct role of the satellite regions in kinetochore recruitment and assembly (Earnshaw, 2015). The surrounding region, the pericentromeric heterochromatin (PCH), has less ordered repeats (233-bp repeat length), termed the major satellite (MajSAT) repeats (Guenatri et al., 2004; Probst et al., 2010).

It has been recognized that despite being highly condensed and lacking genes, centromeric DNA is transcriptionally active (Talbert and Henikoff, 2018; Rošić et al., 2014; Grenfell et al., 2016; Perea-Resa and Blower, 2017, 2018). Such centromeric DNA transcription has recently been reported to be required for the maintenance of centromeric cohesion in human cells (Chen et al., 2021). The centromeric transcripts are long noncoding RNA and termed "centromeric RNA" (Cen-RNA; Gent and Dawe, 2012). The Cen-RNAs are observed at the centromere and are required for kinetochore assembly in mitosis (Ling and Yuen, 2019; Talbert and Henikoff, 2018; Rošić et al., 2014). Cen-RNAs have been observed in the nucleoli of human cells, along with the foundational kinetochore proteins CENPA and CENPC (centromeric protein C), whose deposition is dependent on the presence of Cen-RNAs (McNulty et al., 2017; Perea-Resa and Blower, 2017; Wong et al., 2007). The recruitment of the chromosomal passenger complex is also reported to be Cen-RNA–dependent in both human and mouse cell lines (Smurova and De Wulf, 2018; Ferri et al., 2009; Ideue et al., 2014).

The function of Cen-RNAs has only been investigated so far in somatic cells (Smurova and De Wulf, 2018; Ideue and Tani, 2020), and so nothing is currently known about the function of Cen-RNAs in female meiosis I. This is an important omission given that in this reductional division, sister chromatids are uniquely cosegregated, and mammalian oocytes are associated with a high incidence of mis-segregation (Capalbo et al., 2017; Gruhn et al., 2019; Ottolini et al., 2015; Nagaoka et al., 2012). Although fully grown oocytes are transcriptionally silent, RNAs

[1]Department of Central Laboratory, Clinical Laboratory, Jing'an District Centre Hospital of Shanghai, Shanghai Key Laboratory of Medical Epigenetics, International Laboratory of Medical Epigenetics and Metabolism and Institutes of Biomedical Sciences, the State Key Laboratory of Genetic Engineering, Fudan University, Shanghai, China; [2]Faculty of Engineering and Physical Sciences, University of Southampton, Southampton, UK; [3]School of Biological Sciences, Faculty of Environmental and Life Sciences, University of Southampton, Southampton, UK; [4]Discipline of Obstetrics and Gynecology, School of Medicine, Robinson Research Institute, University of Adelaide, Adelaide, Australia; [5]Genome Damage and Stability Centre, School of Life Sciences, University of Sussex, Brighton, UK.

Correspondence to Tianyu Wu: ty_wu@fudan.edu.cn; Keith T. Jones: keith.jones@sussex.ac.uk.

are transcribed in growing oocytes and maintained during maturation and fertilization (Seydoux and Braun, 2006; DeJong, 2006). Furthermore, maternal RNAs have been demonstrated to be essential for meiosis progression in mouse oocytes (Balboula et al., 2017). Consequently, here we have investigated the function of Cen-RNAs in mouse oocytes and go on to show that they protect the structural integrity of PCH in meiosis I.

Results and discussion

Loss of Cen-RNA induces meiotic arrest in mouse oocytes

To confirm the existence of Cen-RNA in mouse oocytes, we probed for MinSAT RNAs by RNA FISH (Fig. S1 A). We examined transcripts in both orientations (forward and reverse) because both of them were detected in murine cells (Bouzinba-Segard et al., 2006). It was observed that the level of forward transcripts was nearly double that of reverse transcripts (Fig. S1 B; $P < 0.0001$, *t* test). Therefore, the forward transcripts were investigated as the main Cen-RNA.

We first sought to examine Cen-RNA (MinSAT forward transcripts) levels in mouse oocytes. The RNA levels in germinal vesicle (GV) oocytes, maturing oocytes after GV breakdown (MI), and metaphase II arrested (MII) eggs were assessed by quantitative RT-PCR (qRT-PCR), with specific primers for forward transcripts (Maison et al., 2011). Although levels of Cen-RNA were measured to vary between GV, MI, and MII oocytes, these changes were not statistically significant (Fig. S1 C; 95% confidence interval, MI: 0.88-1.66; MII: 0.94-1.29; $n = 3$).

To understand the role of Cen-RNA in mouse female meiosis, an antisense oligonucleotide (ASO) was designed to knock down MinSAT transcripts (Fig. 1 A; Ideue et al., 2014). To test the efficacy of the ASO (Cen-ASO), GV oocytes were microinjected with Cen-ASO or a control ASO containing five bases that were mismatched (5MM-ASO). Following an 18 h incubation, the oocytes were used to generate cDNA. It was observed that 20 or 40 µM Cen-ASO, but not the control 5MM-ASO (40 µM), reduced the long noncoding RNA levels by about half, and a further increase to 100 µM Cen-ASO resulted in a near total loss of MinSAT transcripts (only 4% remaining; Fig. 1 B). The transcript depletion efficacy of Cen-ASO was also confirmed by RNA FISH (Fig. S1, A and B; $P < 0.0001$, *t* test).

The role of Cen-RNA in meiosis was then examined in mouse oocytes. Oocytes were injected with Cen-ASO or 5MM-ASO, arrested for 18 h, and then initiated to resume meiosis. They were scored for completion of MI by polar body extrusion at 15 h after GV breakdown (nuclear envelope breakdown [NEBD]). MinSAT RNA depletion was observed to lower significantly the completion of MI using 20 or 40 µM Cen-ASO (88% maturation using a water injection control versus 75% or 53%, respectively, with Cen-ASO; Fig. 1 C; $P < 0.0001$, χ^2 test), and meiosis I was completely blocked by 100 µM Cen-ASO (0% maturation, $P < 0.0001$, χ^2 test; Fig. 1 C). In contrast, the control 5MM-ASO had no significant effects compared with water injection (90%, $P = 0.542$, χ^2 test; Fig. 1 C). Additionally, depletion of MajSAT transcripts by a similar ASO approach, had no effect on MI completion (85% versus 84%, ns, χ^2 test; Fig. S1, D–F). The results suggest that MinSAT RNAs are required for MI completion in mouse oocytes.

SAC is activated by Cen-RNAs depletion

The SAC is active in mouse oocytes and can arrest them at MI in response to spindle perturbations, chromosome congression, and kinetochore attachment defects, as well as DNA damage (Collins et al., 2015). To determine if the meiotic arrest observed with Cen-RNAs depletion was SAC mediated, Cen-ASO–microinjected oocytes were treated with reversine, a kinase inhibitor of the critical SAC component Mps1 (Santaguida et al., 2010). We and others have previously reported on the ability of reversine to prevent SAC signaling in MI mouse oocytes (El Yakoubi et al., 2017; Lane and Jones, 2014). Most of the oocytes arrested in MI by Cen-ASO completed meiosis when incubated with 100 nM reversine (maturation rates increased from 53% to 95%, χ^2 test, $P < 0.0001$; Fig. 1 C), suggesting that the arrest had been due to SAC activation. To exclude other defects involved in MI arrest, oocytes injected with Cen-ASO or H_2O were treated with reversine (100 nM) from NEBD, a procedure that induced similar timing of anaphase onset for both injected groups ($P > 0.05$, ANOVA; Fig. 1, D and E).

To confirm the MI arrest was SAC dependent, anaphase promoting complex (APC) activity was monitored during oocyte maturation. The APC is an E3 ubiquitin ligase whose substrates, targeted for degradation through ubiquitination, include cyclin B1 and securin (Pesin and Orr-Weaver, 2008). The ability of the SAC to arrest cells, including oocytes during meiosis I, before undergoing anaphase is due to it inhibiting the APC and so preventing loss of cyclin B1 and securin (Herbert et al., 2003). We and others have previously shown that securin degradation can be visualized in real time by coupling to a fluorescent protein during oocyte maturation over several hours preceding polar body extrusion (Homer et al., 2005; Collins et al., 2015). Therefore, GV oocytes were coinjected with securin coupled to YFP and either Cen-ASO or 5MM-ASO. Securin degradation, culminating in extrusion of a polar body, was observed in oocytes microinjected with 5MM-ASO (Fig. 1, F and G). In contrast, oocytes coinjected with Cen-ASO showed no such decrease in securin-YFP fluorescence for the entirety of recording. Securin levels continued to rise, we presume, as a result of insufficient APC activity caused by the maintenance of high SAC activity (Fig. 1 F). To test this, Cen-ASO–injected oocytes were treated with reversine at 6 h after NEBD. A rapid decline of securin fluorescence was observed, which led to extrusion of first polar body (Fig. 1, F and G). Collectively these results support the hypothesis that the depletion of Cen-RNAs induces MI arrest by activating the SAC.

Cen-RNAs are required for proper bivalents alignment

To understand the reason for Cen-RNA depletion–induced SAC activation, we examined the alignment of bivalents during meiosis I. Histone H2B-mCherry and a fluorescent transcription activator-like effector (TALE) against MajSAT repeats (Maj.Sat-mClover) were expressed to track bivalents by high temporal resolution confocal microscopy during meiosis I (Fig. 2 A). By comparison with our previous data (Wu et al., 2018), the time for MI completion was not affected by 5MM-ASO, but it was significantly extended by Cen-ASO (mean time from 9.3 h to 11.6 h, $P < 0.0001$, *t* test; Fig. 2, A and B; and Video 1), suggesting that anaphase was delayed by Cen-RNA depletion.

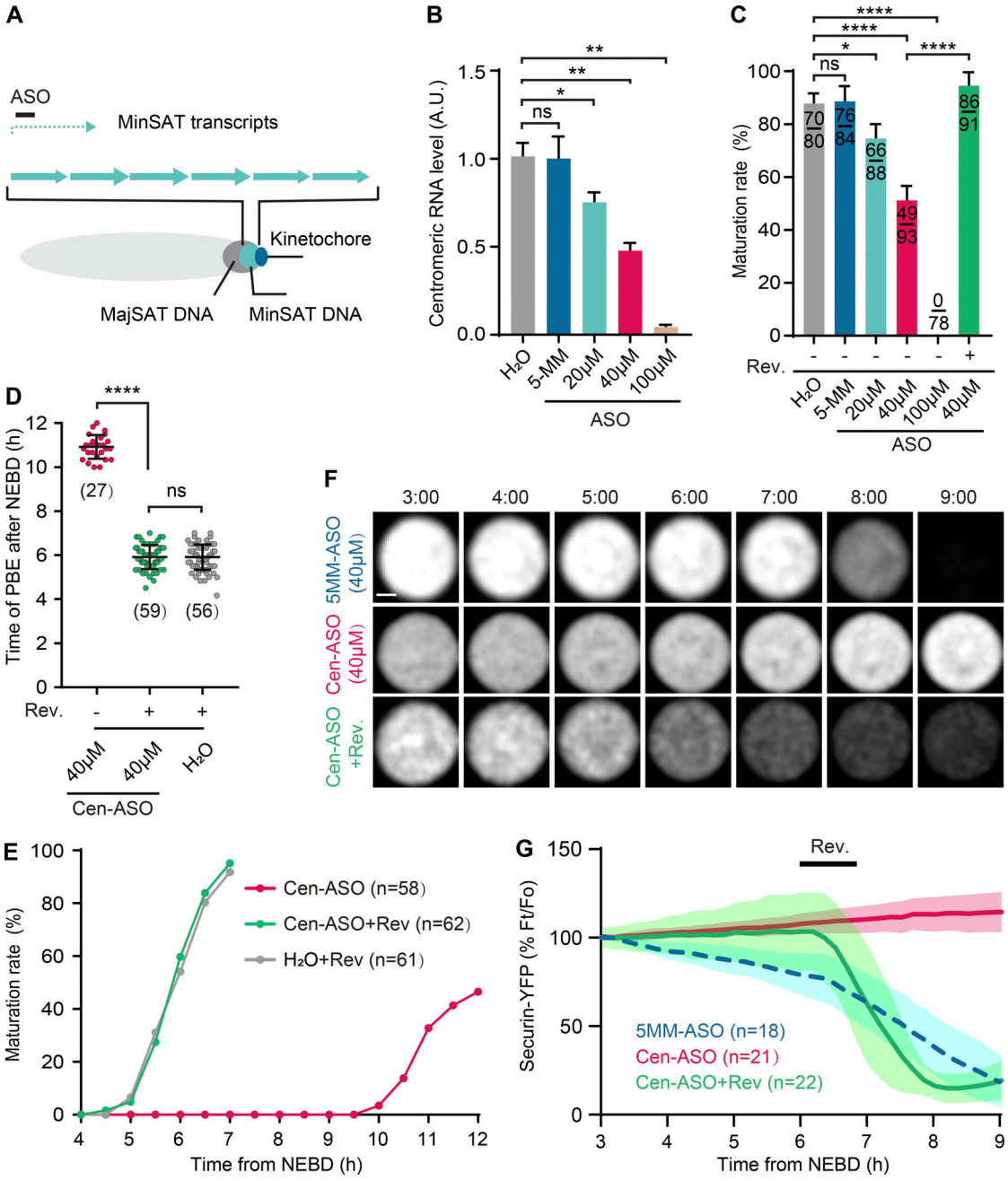

Figure 1. **Oocyte MI completion is prevented by the loss of Cen-RNA. (A)** A Cen-ASO was designed against the MinSAT transcripts. **(B)** The knockdown efficiency of Cen-ASO was tested by qRT-PCR (Cen-ASO: 20, 40, and 100 µM; 5MM-ASO: 40 µM). Analysis of qRT-PCR from three independent experiments (*, $P < 0.05$; **, $P < 0.01$; 95% confidence interval, 5-MM: 0.86-1.14; 20 µM: 0.68-0.82; 40 µM; 0.35-0.61; 100 µM: 0.01-0.07). 30 oocytes in each group. **(C)** Percentage maturation rate following Cen-ASO injection at concentrations indicated, or with water or 5MM-ASO (*, $P < 0.05$; ****, $P < 0.0001$; χ^2 test). Error bars indicate SD. **(D)** The timing of first polar body extrusion (PBE) in Cen-ASO–injected oocytes, as indicated, with reversine (100 nM) added at NEBD (****, $P < 0.0001$; ANOVA with Tukey's post hoc test). Error bars indicate SD. **(E)** Timing of meiotic maturation in oocytes injected as labeled. **(F)** Representative time-lapse images of securin-YFP (gray) expression in oocytes injected with Cen-ASO or 5MM-ASO. Reversine (100 nM) was added at 6 h after NEBD. Scale bar: 20 µm. Times are from NEBD. **(G)** Securin degradation rates (securin-YFP intensity compared with initial time point, Ft/F0) in 5MM-ASO– and Cen-ASO–injected oocytes. Reversine was added as in F. The number of oocytes analyzed in three independent experiments is indicated. Error bars are SD.

To test if Cen-RNA was being synthesized after NEBD or was maternally stored, oocytes were treated with the selective RNA polymerase II inhibitor α-amanitin. We found that the timing of completion of meiosis I is completely unaffected by inhibition of transcription, consistent with recent work (Fig. 2, A and B; and Fig. S1 G; Swartz et al., 2019). As such, we conclude that the effects being observed here are due to loss of maternally stored Cen-RNA.

Bivalent congression on the metaphase plate is usually well advanced at 6 h after NEBD. The alignment and congression of bivalents were therefore evaluated at this time using three parameters: inter-kinetochore distance (Fig. S2 A), distance of

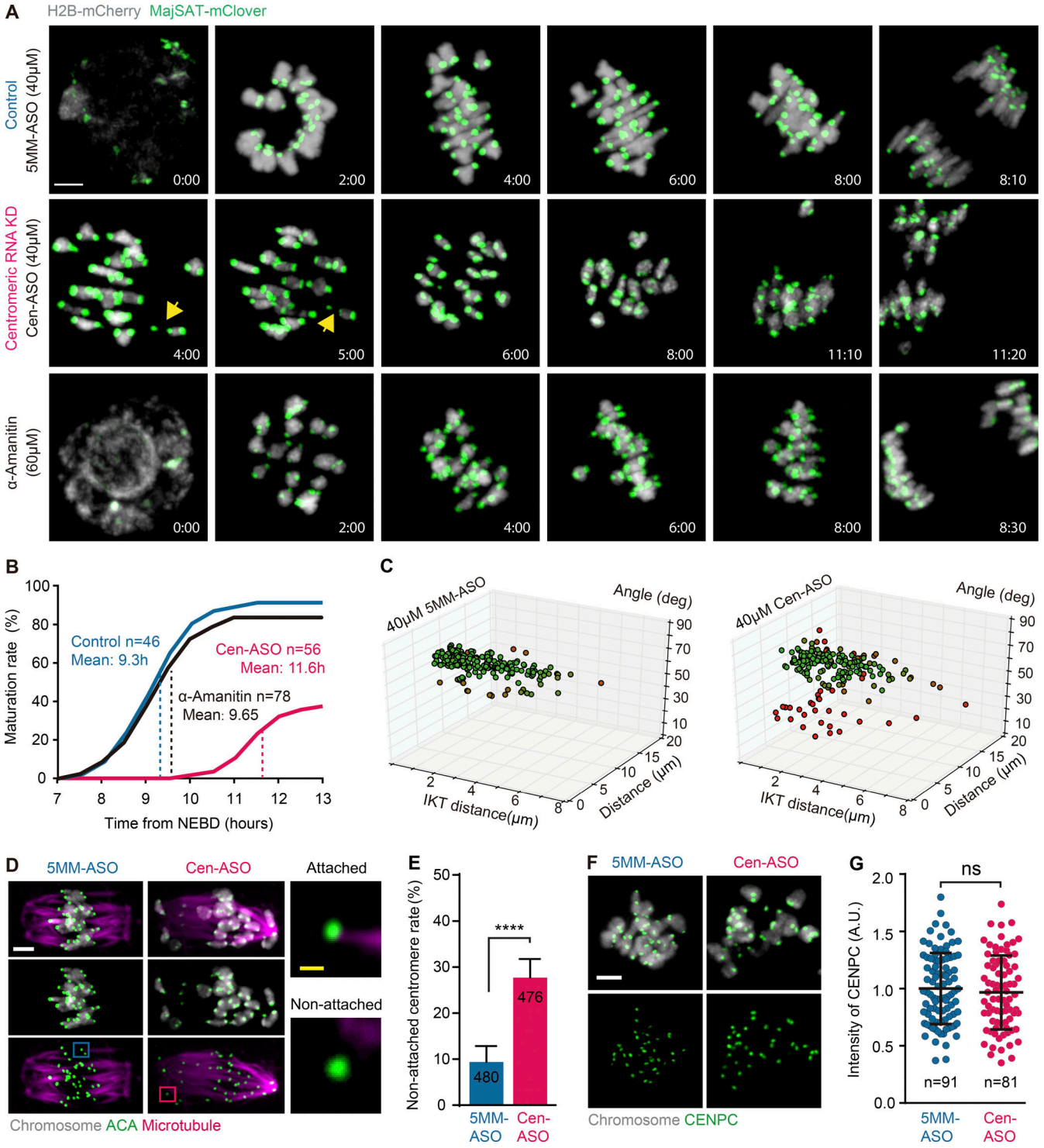

Figure 2. **MI arrest is induced by K-Mt attachment defects. (A)** Representative time-lapse images of oocytes expressing H2B-mCherry (gray) and MajSAT-mClover (green; see Video 1). Damaged centromeres were labeled by yellow arrows; time from NEBD. Scale bar: 5 μm. **(B)** Maturation rates and the mean time for anaphase were measured in A. **(C)** Evaluation of bivalent alignment levels at 6 h after NEBD. 200 bivalents (10 oocytes) were captured by time-lapse imaging for each group. Green: aligned bivalents; red: non-aligned bivalents. IKT distance, inter-kinetochore distance; deg, degree of bivalent angle. The detailed measurement methods are described in Fig. S2. **(D)** K-Mt attachments were detected by immunofluorescence after cold treatment. The attached and nonattached kinetochores are indicated by the blue and red boxes. ACA, anticentromere antibody Scale bar: 5 μm (white); 1 μm (yellow). **(E)** The percentage of nonattached centromeres, from D, was measured (****, $P < 0.0001$, χ^2 test). **(F)** CENPC localization by immunofluorescence. Scale bar: 5 μm. **(G)** CENPC intensity, from F, with background subtraction. Data are normalized with respect to the mean intensity of 5MM-ASO (*t* test). All data from three independent experiments. Error bars indicate SD.

bivalent from the spindle midzone (alignment; Fig. S2 B), and bivalent angle with respect to the spindle long axis (angle; Fig. S2 C; Lane and Jones, 2017; Collins et al., 2015). With 5MM-ASO treatment, bivalents showed a high degree of alignment (Fig. 2 A). Quantification reflected this, with bivalent being clustered with high inter-kinetochore distance, low alignment distances, and high angle scores (green points, Fig. 2 C; and Fig. S2, A–C). In contrast, for Cen-ASO treatment, bivalents were visibly further from the metaphase plate, and with greater spread in the evaluation (red points, Fig. 2 C; and Fig. S2, A–C).

In addition to the delayed or blocked completion of meiosis I, chromosomal defects were observed in oocytes microinjected with Cen-ASO. This included nonaligned bivalents during congression, as well as lagging chromosomes during anaphase (Fig. 2 A; and Fig. S2, D–G).

Importantly, the splitting of centromere signals was observed with Cen-ASO (Fig. 2 A, arrow) but not with 5MM-ASO. Such splitting of the centromere signal was not an artifact associated specifically with the Cen-ASO because an siRNA designed to deplete MinSAT RNAs, which had good efficacy in doing this (Fig. S1, H–J) and which raised rates of MI arrest (Fig. S1K), was also observed to induced pericentromeric DNA damage (Fig. S1, L and M).

We hypothesized that the observed cleavage of centromeres would affect the ability to form correct kinetochore–microtubule (K-Mt) attachments. To examine this, oocytes were cold-treated and fixed at 6 h after NEBD to assess K-Mt attachment (Fig. 2 D). As expected, significantly greater K-Mt attachment defects (Fig. 2 D) were observed with Cen-ASO compared with 5MM-ASO (28.2% versus 8.3%, $P < 0.0001$, χ^2 test; Fig. 2 E). However, the intensity of CENPC, measured by immunofluorescence, was not affected ($P > 0.05$, t test; Fig. 2, F and G), suggesting that the kinetochore had not lost its basic integrity.

The alignment defects are induced by damaged centromeres

To ascertain the reason for K-Mt attachment defects, the integrity of centromeres was further evaluated in MI oocytes. Oocytes expressing MajSAT-mClover to label PCH were fixed and examined for histone 2AX phosphorylated on serine 139 (γH2AX), which marks DNA double strand breaks (DSBs; Collins et al., 2015). We found only γH2AX signals on bivalents following Cen-ASO injection (0% versus 33.9%, χ^2 test, $P < 0.0001$; Fig. 3, A and B). Furthermore, γH2AX was specifically concentrated at the damaged centromeres (Fig. 3 A, red box). Such accumulation of γH2AX following DSBs, leading to SAC activation, has previously been reported (Collins et al., 2015; Lane et al., 2017).

We evaluated the ability of bivalents with damaged centromeres, which was assessed by a diminished MajSAT intensity in one of their two sister chromatid pairs, to align on the spindle. It was observed that damaged bivalents can only be attached to microtubules through their sister chromatid pair with an intact (i.e., normal MajSAT intensity) centromere, but not the sister chromatid pair with the damaged centromere (Fig. 3, C and D). In further analysis, we evaluated the alignment level of such damaged bivalents (as previously performed in Fig. 2 C). Such analysis revealed far less alignment of damaged bivalents, with diminished MajSAT intensity (Fig. 3 E). Indeed, when compared with those intact, bivalents with damaged centromeres had lower levels of tension (Fig. 3 F), were further from the spindle midzone (Fig. 3 G), and were less likely to be orientated properly on the spindle (Fig. 3 H). These results suggest that poor alignment of bivalents is associated with damaged centromeres.

To confirm that the SAC was activated by the damaged centromere, we probed for Mad2 immunofluorescence in oocytes 6 h after NEBD. Consistently, Mad2 was found primarily on damaged centromeres rather than on the intact centromeres (91% versus 14%, $P < 0.0001$, χ^2 test; Fig. 3, I and J).

Unstable PCH is split by the tension from microtubules

To determine how the centromeres were damaged, we used mCherry-CenpC to label the inner kinetochore, in addition to MajSAT-mClover, and Hoechst to label chromatin (Fig. 4 A). In oocytes injected with Cen-ASO, splitting of the centromere was observed within the MajSAT-mClover signal but not the mCherry-CenpC signal (Fig. 4, A and B). These observations suggest that the region of the MajSAT and not the MinSAT is split.

To confirm our hypothesis, we examined the centromere closely in oocytes coinjected with cRNA (cloned RNA) constructs encoding fluorescently labeled TALEs against the MinSAT (mRuby) and MajSAT (mClover) regions separately (Fig. 4 B). Live cell imaging was performed at 6 h after NEBD. We found Cen-RNA knockdown was associated with stretching and breaking of the MajSAT region, but with no observable effect on the inner kinetochore (CENPC) or MinSAT region ($P < 0.0001$, ANOVA, $n = 127$; Fig. 4, B and C). Furthermore, the signals were found to separate into two parts in real-time imaging (Fig. S3 A), with the breaking point corresponding with that seen in the PCH (MajSAT DNA; Fig. S3 B). Meanwhile, we found more damaged centromeres than stretched centromeres at 6 h after NEBD (Fig. 4 C), inferring that centromeres were broken before metaphase was reached.

3D time-lapse imaging was performed on Cen-ASO–injected oocytes, expressing MajSAT-mClover and H2B-mCherry (Fig. 4 D). Fragmented PCH at most time points was observed (Fig. 4 E). Observation of the MajSAT-mClover signals as they split into two fragments happened gradually over tens of minutes, and the two fragments could stay in proximity for several hours (Video 2). The time-lapse analysis identified around six damaged centromeres per oocyte, with the first ones appearing within an hour of NEBD, and the last being complete 3–4 h later ($P < 0.0001$, ANOVA; Fig. 4 F), coincident with early meiotic spindle formation and the first establishment of K-Mt interaction (Kitajima et al., 2011; Brunet et al., 1999).

It is hypothesized that microtubule tension across the bivalents generated the necessary force to cause fragmentation. Therefore, the time-lapse experiments were repeated, but with the addition of monastrol, a KIF11 inhibitor, which collapses the spindle onto a single pole and prevents tension generation across the chromosomes. This intervention significantly reduced the frequency of fragmented PCH ($P < 0.0001$, ANOVA; Fig. 4, D and G). These observations support the hypothesis that PCH without the presence of Cen-RNA is prone to be broken through tension generated from microtubules (Fig. 4 H).

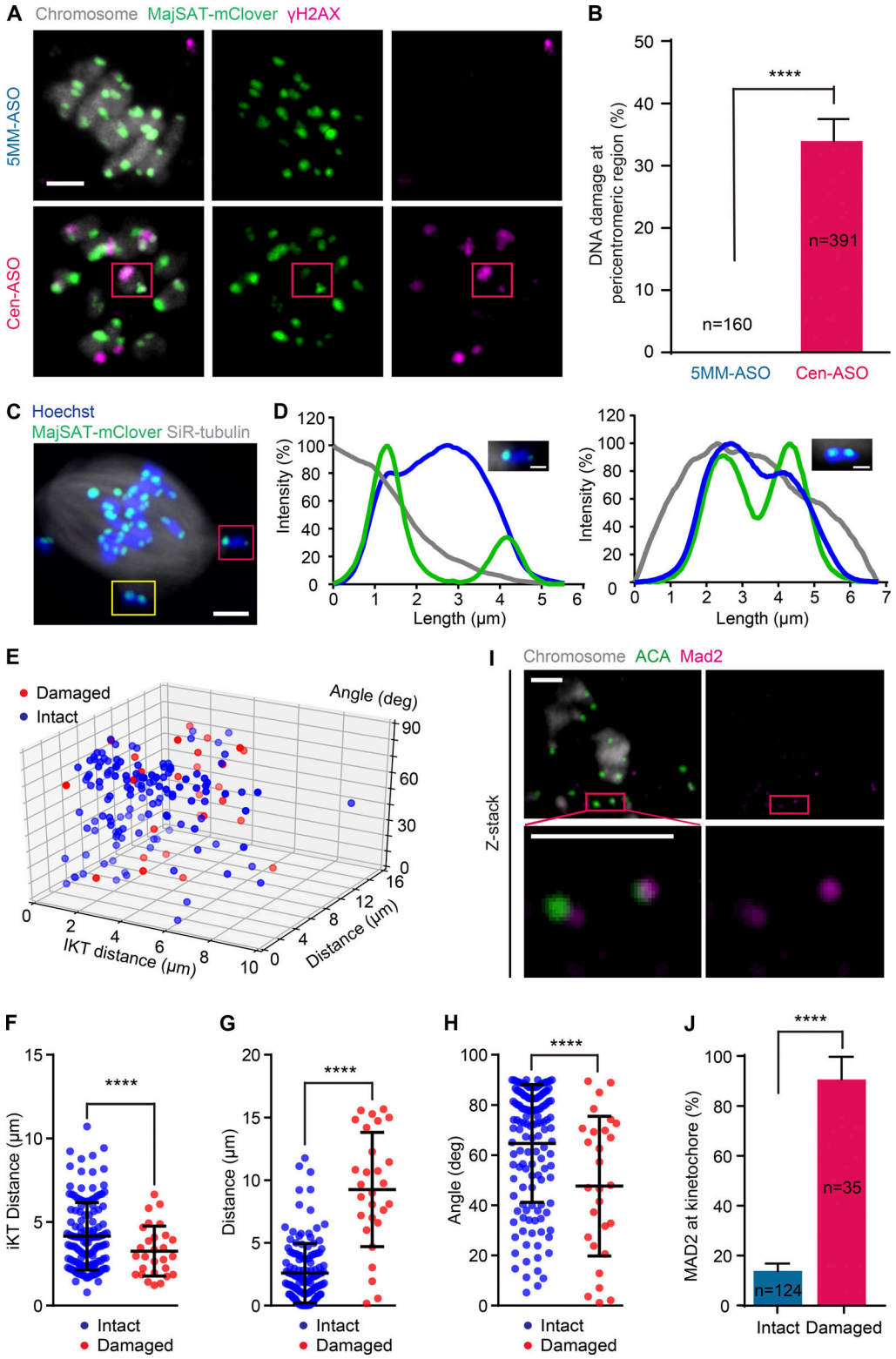

Figure 3. **Centromere damage occurs in PCH. (A)** Representative images showing γH2AX staining in oocytes 6 h after NEBD, treated with 40 μM Cen-ASO or 5MM-ASO. Damaged centromeres indicated by red boxes. Scale bar: 5 μm. **(B)** Percentage of centromeres containing DSBs, as assessed from γH2AX staining data in A ($P < 0.0001$, χ^2 test; three independent experiments). **(C)** Representative image showing nonaligned bivalents with (red) and without (yellow) damaged centromeres, as assessed by the loss of MajSAT signal in one of the two sister chromatid pairs. Scale bar: 5 μm. **(D)** Line intensity plots of the MajSAT-mClover (green), tubulin (gray), and chromatin (blue) of bivalents indicated in C. Scale bar: 2 μm. **(E)** Bivalents with damaged ($n = 28$) or intact centromeres ($n = 138$) were analyzed individually and evaluated for three different measurements of alignment (166 bivalents from 10 oocytes). IKT distance, inter-kinetochore distance; deg, degree of bivalent angle. **(F–H)** The inter-kinetochore distance (F), alignment distance (G), and angle (H) were compared between bivalents with (red) and without (blue) damaged centromeres (****, $P < 0.0001$, *t* test). **(I)** Representative image to show kinetochore and Mad2 immunofluorescence in an

oocyte injected with Cen-ASO. The damaged centromeres with Mad2 were shown in red boxes (enlarged version at the bottom). ACA, anticentromere antibody. Scale bars: 5 µm. **(J)** The percentage of kinetochores containing Mad2 in I, compared between centromeres that were either intact or damaged (****, $P < 0.0001$, χ^2 test). Data from three independent experiments. Error bars indicate SD.

In summary, we have investigated the specific role of MinSAT transcripts in mouse oocytes during meiosis I. These Cen-RNAs are likely to be transcribed and maintained at the centromere before oocyte maturation. It is concluded that Cen-RNA appears to play a structural role in protecting MajSAT DNA at PCH. These effects seem specific, as DNA damage was observed using both an ASO and an siRNA approach to Cen-RNA, but not using a five-base ASO mismatch, nor were they seen following knockdown of MajSAT transcripts. Following a reduction in Cen-RNA brought about by Cen-ASO, MajSAT DNA can be split by the tension from microtubules. The damaged bivalents recruit γH2AX and are not aligned properly at the metaphase plate. Therefore, the DNA damage and isolated kinetochores induce SAC activation, lower APC activity, and so prevent the completion of meiosis I (Fig. 5). As such, these findings show a novel, surprising, and necessary function of Cen-RNA for the completion of meiosis I.

The localization of MinSAT RNAs at centromeric and pericentromeric regions has been reported in murine cells (Huo et al., 2020; Bouzinba-Segard et al., 2006; Ferri et al., 2009); however, the situation is currently unclear in human cells. Although previous reports of human Cen-RNAs at the centromeres have been made (Ideue et al., 2014; McNulty et al., 2017), a recent investigation showed a dissociation of the majority of Cen-RNAs from the centromere during mitosis (Bury et al., 2020). Furthermore, Cen-RNAs are thought to be transacting at the centromeres of yeast (Ling and Yuen, 2019); however, Cen-RNAs stay in cis in human cells (McNulty et al., 2017). These observations point to the localization and behavior of Cen-RNAs that may well be cell stage– and species-specific.

It is assumed that MinSAT RNA that had been transcribed before oocyte maturation must stay at the centromere, and somehow protect the MajSAT DNA at the PCH. We suggest three possible roles for Cen-RNAs during cell division: (1) it is a structural component of the PCH, (2) it recruits such a component, or (3) it encodes such a component. We favor the first two possibilities given these RNAs are thought to be noncoding. There are a number of possible mechanistic ways, not examined here, of how MinSAT RNA could protect PCH.

Notably, Cen-RNA has been observed at the MajSAT region, and the composition of such a structure is partially revealed. A recent study provided one such scenario by showing that the nuclear matrix protein SAFB, through interaction with both MinSAT and MajSAT RNAs, localized to PCH in mouse cells. Loss of SAFB localization resulted in chromatin changes that likely were caused by decondensation of PCH (Huo et al., 2020). Therefore, Cen-RNAs may also cooperate with SAFB to protect PCH in mouse oocytes through phase separation. Although we have identified the potential role of Cen-RNAs at PCH during meiosis, the molecular basis of this remains to be investigated.

Damaged centromeres, with cleavage in the pericentromeric region, have been observed in cancer cell lines such as those deriving from colorectal carcinomas or adenocarcinomas. However, the players in this centromere fragility are presently unclear (Barra and Fachinetti, 2018). Additionally, centromere splitting has been observed in aged oocytes (Zielinska et al., 2019). Such observations, based on the data presented here, may be related to Cen-RNA depletion. In conclusion, the need of Cen-RNA for PCH stability in mouse MI oocytes may be a factor in the high rates of aneuploidy in eggs associated with maternal aging, and more widely in the susceptibility of chromosomes to rearrangements brought about by DNA breakage.

Materials and methods

All reagents were from Sigma-Aldrich unless otherwise stated.

Animals and oocyte culture

All mice were used in accordance with local and UK government regulations on the use of animals in research. 3–4-wk female C57Bl/6 mice were used. GV oocytes were released from the ovaries 44–52 h following hormonal priming with 10 IU Pregnant Mare Serum Gonadotropin by intraperitoneal injection (Centaur Services). Milrinone (1 µM) was added to M2 medium to maintain oocyte prophase arrest. Oocytes were stripped from the surrounding cells mechanically. For maturation, GV oocytes were washed free from milrinone and cultured in fresh M2 media on heat block.

qRT-PCR

Total RNA from oocytes was extracted with the RNeasy Mini Kit (QIAGEN). Reverse transcription was performed with the SuperScript IV First-Strand Synthesis System (Cat. 18091200). The cDNA was synthesized with forward (For)-specific primers for MinSAT or MajSAT RNAs (Maison et al., 2011). qRT-PCR was performed with SYBR Premix Ex Taq (Takara; Cat. RR420A). Primers for MinSAT RNA were (For) 5′-GAAAATGATAAAAAC CACAC-3′ and reverse (Rev) 5′-ACTCATTGATATACACTGTT-3′. Analysis was performed using the $_{\Delta\Delta}$CT method with GAPDH as the reference transcripts. Primers for MajSAT RNA were (For) 5′-AAATACACACTTTAGGACG-3′ and (Rev) 5′-TCAAGTGGA TGTTTCTCATT-3′. Primers for GAPDH (standard) were (For) 5′-CAAATTCCATGGCACCGTCA-3′ and (Rev) 5′- GGCAGAGAT GATGACCCTTT-3′.

Microinjection

Oocytes were microinjected in a 37°C heated chamber (Intracel) on the stage of an inverted TE300 microscope (Nikon) with micromanipulators (Narishige). A 0.1–0.3% volume of cRNA was injected using a timed pulse on a Pneumatic Picopump (World Precision Instruments) using pipette RNA concentrations as follows: securin-YFP (500 ng/µl), TALE MajSAT-mClover (600 ng/µl), and TALE MinSAT-mRuby, H2B-mCherry (500 ng/µl). cRNAs were centrifuged for 5 min at 16,000 *g* before micro-injection.

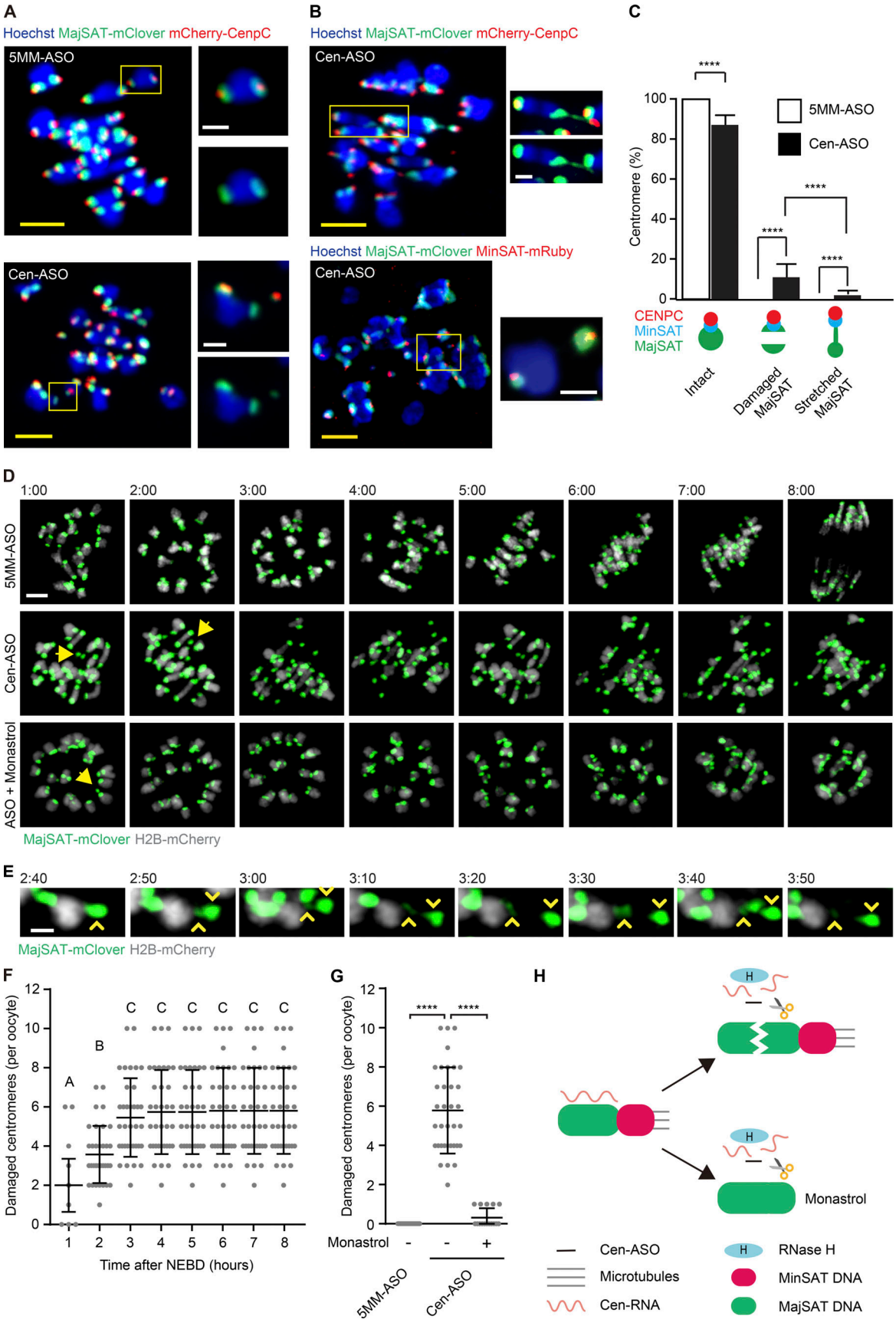

Figure 4. **Centromere damage is microtubule tension–dependent. (A and B)** Representative images show centromeres in oocytes treated with 40 µM 5MM-ASO or Cen-ASO. Yellow boxes indicate the bivalents enlarged in the inset (blue: Hoechst; green: MajSAT-mClover; red: MajSAT-mRuby or mCherry-

CenpC). Scale bars: 5 µm (yellow) and 2 µm (white). **(C)** The proportion of centromeres classified by damage location in B (287 bivalents were imaged at 6 h after NEBD; data from three independent experiments; ****, P < 0.0001, ANOVA with Tukey's post hoc test). **(D)** Representative time-lapse images showing the time of centromere damage initiation (gray: H2B-mCherry; green: MajSAT-mClover). Monastrol was added at the beginning of oocyte maturation in culture. Yellow arrow: damaged centromeres. Time from NEBD. Scale bar: 5 µm. **(E)** Time-lapse images show the process of a single representative centromere signal splitting (gray: H2B-mCherry; green: MajSAT-mClover; yellow arrows: paired centromere signals; Video 2). Time from NEBD. Scale bar: 2 µm. **(F)** Number of damaged centromeres per oocyte are plotted by time (A versus B, P = 0.0235; B versus C, P = 0.0023; A versus C, P < 0.0001; ANOVA with Tukey's post hoc test). 35 oocytes were tested in three independent experiments. **(G)** Number of damaged centromeres per oocyte (5MM-ASO: *n* = 29; Cen-ASO: *n* = 35; monastrol: *n* = 16; ****, P < 0.0001, ANOVA with Tukey's post hoc test). **(H)** Schematic showing the mechanism of MajSAT DNA damage. The Cen-ASO activates RNaseH, which cleaves the DNA–RNA heteroduplex and therefore leads to degradation of Cen-RNA, inducing the instability of centromeric DNA. Data from three independent experiments. Error bars indicate SD.

RNA interference

The Cen-RNA was knocked down by ASOs and siRNAs in different concentrations (Eurofins). The sequence for Cen-ASO was mU*mG*mU*mU*mU*T*T*C*A*G*T*G*T*A*A*mC*mU*mC*mA*mC. The sequence of specific 5MM-ASO was mU*mG*m**A***m**A***mU*T***A*C*A*G*T*G***A*A*A*mC*m**A***mC*mA*mC (mismatched nucleotides were marked with bold and underline). The sequence for siRNA was GGAAACGGGAUUUGUAGAATT. The ASO to deplete MajSAT transcripts was designed against MajSAT RNAs: mC*mA*mG*mU*mU*T*T*C*T*T*G*C*C*A*T*mA*mU*mU*mC*mC. The control sequence also with five mismatches was mC*mA*mG*m**A***mU*T***A*C*T***A*G*C*C*A***A*mA*mU*m**A***mC*mC. The "m" represents 2′-O-methoxyethylribonucleotide. An asterisk represents a phosphorothioate bond.

cRNA manufacture

cRNA was transcribed in vitro from purified linear double-stranded DNA templates. mMessage T7 or T3 RNA polymerase kits (Ambion, Life Technologies) were used for the in vitro transcription reaction (Lane et al., 2012). cRNA was suspended in nuclease-free water, and the concentration of RNA products was determined by photo spectroscopy. MinSAT-mRuby and MajSAT-mClover were gifts from Dr. Maria-Elena Torres-Padilla (Institute of Epigenetics and Stem Cells, Munich, Germany; Addgene plasmids #47880 and #47878, respectively; Miyanari et al., 2013; Thanisch et al., 2014), which bind to the MinSAT and MajSAT DNA directly. Securin-YFP was made by cloning securin into a modified pRN3 plasmid containing the YFP using restriction digests and ligation. H2B-mCherry was made in the same way. mCherry-CenpC was a gift from Dr. Jan Ellenberg (European Molecular Biology Laboratory, Heidelberg, Germany; Euroscarf; #P30660).

Time-lapse imaging

Time points were acquired at 10-min intervals using a Leica SP8 fitted with hybrid detectors, an environmental chamber set to 37°C, and either a 40×/1.3 NA or a 63×/1.4 NA Plan Apochromat oil immersion lens. In-laboratory software written in Python language was used to image multiple-stage regions and to track chromosomes in up to 30 oocytes per experiment, using H2B-mCherry signal to ensure bivalents remained in the center of an ∼32 × 32 × 32–µm imaging volume.

Immunofluorescence microscopy

Oocytes were fixed for 30 min in PBS containing 2% formaldehyde and 0.05% Triton X-100, and were then permeabilized for 15 min in PBS containing 0.05% Triton X-100. Fixing and permeabilizing were performed at room temperature, and oocytes were extensively washed with PBS between stages. Oocytes were incubated at 4°C overnight in a blocking buffer of 7% goat serum in PBS supplemented with 0.05% Tween-20. Primary antibodies used were γH2AX antibody (Abcam; ab2893; 1:500), Mad2 antibody (Proteintech; 10337–1-AP; 1:200), CENPC antibody (ABclonal; A3975; 1:200), and anti-centromere antibody (ImmunoVision; HCT-0100; 1:500). Secondary antibodies used were goat anti-rabbit Alexa Fluor 488 (Life Technologies; a-21070; 1:500), goat anti-rabbit Cy3 (Abclonal; AS008; 1:500), and goat anti-human Atto 488 (Merck; 52526; 1:500). These incubations were at 37°C in blocking solution for 1 h. Chromatin was briefly counterstained with Hoechst (MCE; HY-15559; 5 µg/ml) before imaging. The samples were in PBS and imaged by Leica SP8 with a 63×/1.4 NA Plan Apochromat oil immersion lens at room temperature.

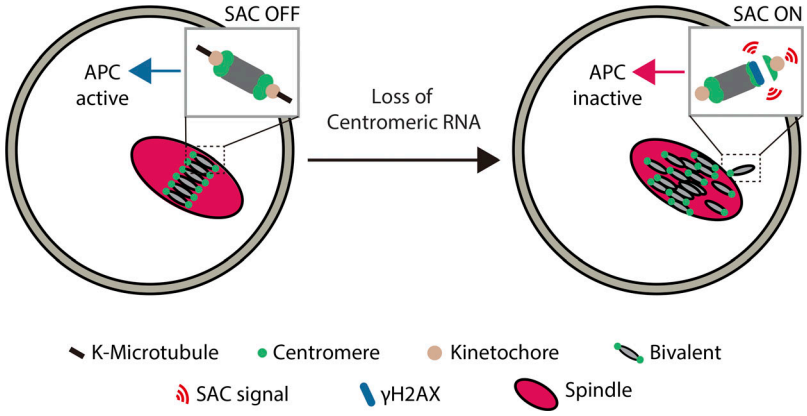

Figure 5. **Loss of Cen-RNA activates SAC by breaking centromeric DNA.** Normally, bivalents are stretched by microtubules at late metaphase and aligned properly at the metaphase plate. The SAC signal is turned off, and the APC is activated for the completion of meiosis I (left). However, Cen-RNAs reduction leads to damaged centromeres and unattached kinetochores (dashed square), which activates the SAC and restrains APC to arrest oocyte at meiosis I (right).

Cold treatment for microtubule depolymerization

Oocytes were placed on ice for 10 min to depolymerize non–K-Mts. Oocytes were immediately fixed following cold treatment and then processed for immunofluorescence as described above.

Inhibitor treatment

Monastrol (10 µM) was added to oocytes from NEBD. Reversine (100 nM) was added from NEBD or 6 h later depending on experiments. α-amanitin (Tocris; Cat. 4025; 60 µM) was added to oocytes from NEBD. SiR-tubulin (1 µM) was added to oocytes from NEBD.

RNA FISH

After permeabilization with 0.5% Triton X-100 in PBS for 5 min on ice, MI oocytes were fixed in 4% paraformaldehyde in PBS for 30 min and stored in 70% EtOH at −20°C overnight. Oocytes were transferred into 2% Triton X-100 for 10 min at room temperature. Following dehydration in 80%, 95%, and 100% EtOH, we performed hybridization with 1 µM locked nucleic acid fluorescent probes (Tsingke) in 10% formamide, 2× SSC, and 10% dextran sulfate in an incubator overnight at 37°C. After three washes in 2× SSC for 5 min at 60°C, oocytes were imaged by confocal microscopy (Susor et al., 2015). The sequence of probe for forward transcripts was 5′-GTTCTACAAATCCCGTTTCC-3′; the sequence of probe for reverse transcripts was 5′-TACACTGAAAAACACATTCG-3′. For RNase treatment, the MI oocytes were treated with 1 mg/ml of RNaseA (Yeasen; 10405ES03) in PBS and incubated for 15 min at room temperature after permeabilization (Maison et al., 2002).

Foci intensity measurement

To find the intensity of kinetochore proteins or centromeric transcripts, we measured the integrate intensity of each focus with ImageJ. The Foci_Picker3D plugin was used to analyze the integrated intensity (only the foci with no overlap in 3D images were measured). The same threshold was applied to each focus within an oocyte.

Statistical analysis

Sample means were compared with either a Student's *t* test, a paired *t* test, or a one-way ANOVA with a post hoc test as stated (two-sided). Data distribution was normal. Dichotomous data were compared using a χ^2 test. Tests were performed using GraphPad Prism 7 (GraphPad Software).

Online supplemental material

Fig. S1 shows results from additional experiments supplementing Fig. 1 and Fig. 2. Fig. S2 and Video 1 show results from additional experiments supplementing Fig. 2. Fig. S3 shows results from additional experiments supplementing Fig. 4. Video 2 shows results from additional experiments supplementing Fig. 4.

Acknowledgments

We thank Dr. Maria-Elena Torres-Padilla for the gifts of the MinSAT-mRuby and MajSAT-mClover constructs Dr. Jan Ellenberg for the mCherry-CenpC construct.

This work was supported by a China Postdoctoral Science Foundation special grant (2020TQ0069) and a China Postdoctoral Science Foundation grant (2020M670985) to T. Wu and a Leverhulme Trust grant (RPG-2017-352) to K.T. Jones.

The authors declare no competing financial interests.

Author contributions: T. Wu, S.I.R. Lane, and K.T. Jones devised the study. T. Wu performed the experiments and analysis. S.L. Morgan and F. Tang helped in the molecular work. The manuscript was written by T. Wu, S.I.R. Lane, and K.T. Jones with input from all authors.

Submitted: 27 November 2020
Revised: 1 May 2021
Accepted: 27 July 2021

References

Balboula, A.Z., C.S. Blengini, A.S. Gentilello, M. Takahashi, and K. Schindler. 2017. Maternal RNA regulates Aurora C kinase during mouse oocyte maturation in a translation-independent fashion. *Biol. Reprod.* 96: 1197–1209. https://doi.org/10.1093/biolre/iox047

Barra, V., and D. Fachinetti. 2018. The dark side of centromeres: types, causes and consequences of structural abnormalities implicating centromeric DNA. *Nat. Commun.* 9:4340. https://doi.org/10.1038/s41467-018-06545-y

Bouzinba-Segard, H., A. Guais, and C. Francastel. 2006. Accumulation of small murine minor satellite transcripts leads to impaired centromeric architecture and function. *Proc. Natl. Acad. Sci. USA.* 103:8709–8714. https://doi.org/10.1073/pnas.0508006103

Brunet, S., A.S. Maria, P. Guillaud, D. Dujardin, J.Z. Kubiak, and B. Maro. 1999. Kinetochore fibers are not involved in the formation of the first meiotic spindle in mouse oocytes, but control the exit from the first meiotic M phase. *J. Cell Biol.* 146:1–12. https://doi.org/10.1083/jcb.146.1.1

Bury, L., B. Moodie, J. Ly, L.S. McKay, K.H.H. Miga, and I.M. Cheeseman. 2020. Alpha-satellite RNA transcripts are repressed by centromere-nucleolus associations. *eLife.* 9:e59770. https://doi.org/10.7554/eLife.59770

Capalbo, A., E.R. Hoffmann, D. Cimadomo, F.M. Ubaldi, and L. Rienzi. 2017. Human female meiosis revised: new insights into the mechanisms of chromosome segregation and aneuploidies from advanced genomics and time-lapse imaging. *Hum. Reprod. Update.* 23:706–722. https://doi.org/10.1093/humupd/dmx026

Chen, Y., Q. Zhang, Z. Teng, and H. Liu. 2021. Centromeric transcription maintains centromeric cohesion in human cells. *J. Cell Biol.* 220: e202008146. https://doi.org/10.1083/jcb.202008146

Collins, J.K., S.I.R. Lane, J.A. Merriman, and K.T. Jones. 2015. DNA damage induces a meiotic arrest in mouse oocytes mediated by the spindle assembly checkpoint. *Nat. Commun.* 6:8553. https://doi.org/10.1038/ncomms9553

DeJong, J. 2006. Basic mechanisms for the control of germ cell gene expression. *Gene.* 366:39–50. https://doi.org/10.1016/j.gene.2005.10.012

Earnshaw, W.C. 2015. Discovering centromere proteins: from cold white hands to the A, B, C of CENPs. *Nat. Rev. Mol. Cell Biol.* 16:443–449. https://doi.org/10.1038/nrm4001

El Yakoubi, W., E. Buffin, D. Cladière, Y. Gryaznova, I. Berenguer, S.A. Touati, R. Gómez, J.A. Suja, J.M. van Deursen, and K. Wassmann. 2017. Mps1 kinase-dependent Sgo2 centromere localisation mediates cohesin protection in mouse oocyte meiosis I. *Nat. Commun.* 8:694. https://doi.org/10.1038/s41467-017-00774-3

Ferri, F., H. Bouzinba-Segard, G. Velasco, F. Hubé, and C. Francastel. 2009. Non-coding murine centromeric transcripts associate with and potentiate Aurora B kinase. *Nucleic Acids Res.* 37:5071–5080. https://doi.org/10.1093/nar/gkp529

Fukagawa, T., and W.C. Earnshaw. 2014. The centromere: chromatin foundation for the kinetochore machinery. *Dev. Cell.* 30:496–508. https://doi.org/10.1016/j.devcel.2014.08.016

Gent, J.I., and R.K. Dawe. 2012. RNA as a structural and regulatory component of the centromere. *Annu. Rev. Genet.* 46:443–453. https://doi.org/10.1146/annurev-genet-110711-155419

Grenfell, A.W., R. Heald, and M. Strzelecka. 2016. Mitotic noncoding RNA processing promotes kinetochore and spindle assembly in Xenopus. *J. Cell Biol.* 214:133–141. https://doi.org/10.1083/jcb.201604029

Gruhn, J.R., A.P. Zielinska, V. Shukla, R. Blanshard, A. Capalbo, D. Cimadomo, D. Nikiforov, A.C.H. Chan, L.J. Newnham, I. Vogel, et al. 2019. Chromosome errors in human eggs shape natural fertility over reproductive life span. *Science.* 365:1466–1469. https://doi.org/10.1126/science.aav7321

Guenatri, M., D. Bailly, C. Maison, and G. Almouzni. 2004. Mouse centric and pericentric satellite repeats form distinct functional heterochromatin. *J. Cell Biol.* 166:493–505. https://doi.org/10.1083/jcb.200403109

Herbert, M., M. Levasseur, H. Homer, K. Yallop, A. Murdoch, and A. McDougall. 2003. Homologue disjunction in mouse oocytes requires proteolysis of securin and cyclin B1. *Nat. Cell Biol.* 5:1023–1025. https://doi.org/10.1038/ncb1062

Homer, H.A., A. McDougall, M. Levasseur, K. Yallop, A.P. Murdoch, and M. Herbert. 2005. Mad2 prevents aneuploidy and premature proteolysis of cyclin B and securin during meiosis I in mouse oocytes. *Genes Dev.* 19: 202–207. https://doi.org/10.1101/gad.328105

Huo, X., L. Ji, Y. Zhang, P. Lv, X. Cao, Q. Wang, Z. Yan, S. Dong, D. Du, F. Zhang, et al. 2020. The Nuclear Matrix Protein SAFB Cooperates with Major Satellite RNAs to Stabilize Heterochromatin Architecture Partially through Phase Separation. *Mol. Cell.* 77:368–383.e7. https://doi.org/10.1016/j.molcel.2019.10.001

Ideue, T., and T. Tani. 2020. Centromeric Non-Coding RNAs: Conservation and Diversity in Function. *Noncoding RNA.* 6:4. https://doi.org/10.3390/ncrna6010004

Ideue, T., Y. Cho, K. Nishimura, and T. Tani. 2014. Involvement of satellite I noncoding RNA in regulation of chromosome segregation. *Genes Cells.* 19:528–538. https://doi.org/10.1111/gtc.12149

Jones, K.T., and S.I.R. Lane. 2013. Molecular causes of aneuploidy in mammalian eggs. *Development.* 140:3719–3730. https://doi.org/10.1242/dev.090589

Kitajima, T.S., M. Ohsugi, and J. Ellenberg. 2011. Complete kinetochore tracking reveals error-prone homologous chromosome biorientation in mammalian oocytes. *Cell.* 146:568–581. https://doi.org/10.1016/j.cell.2011.07.031

Lane, S.I.R., and K.T. Jones. 2014. Non-canonical function of spindle assembly checkpoint proteins after APC activation reduces aneuploidy in mouse oocytes. *Nat. Commun.* 5:3444. https://doi.org/10.1038/ncomms4444

Lane, S.I.R., and K.T. Jones. 2017. Chromosome biorientation and APC activity remain uncoupled in oocytes with reduced volume. *J. Cell Biol.* 216: 3949–3957. https://doi.org/10.1083/jcb.201606134

Lane, S.I.R., Y. Yun, and K.T. Jones. 2012. Timing of anaphase-promoting complex activation in mouse oocytes is predicted by microtubule-kinetochore attachment but not by bivalent alignment or tension. *Development.* 139:1947–1955. https://doi.org/10.1242/dev.077040

Lane, S.I.R., S.L. Morgan, T. Wu, J.K. Collins, J.A. Merriman, E. ElInati, J.M. Turner, and K.T. Jones. 2017. DNA damage induces a kinetochore-based ATM/ATR-independent SAC arrest unique to the first meiotic division in mouse oocytes. *Development.* 144:3475–3486. https://doi.org/10.1242/dev.153965

Ling, Y.H., and K.W.Y. Yuen. 2019. Point centromere activity requires an optimal level of centromeric noncoding RNA. *Proc. Natl. Acad. Sci. USA.* 116:6270–6279. https://doi.org/10.1073/pnas.1821384116

Maison, C., D. Bailly, A.H.F.M. Peters, J.P. Quivy, D. Roche, A. Taddei, M. Lachner, T. Jenuwein, and G. Almouzni. 2002. Higher-order structure in pericentric heterochromatin involves a distinct pattern of histone modification and an RNA component. *Nat. Genet.* 30:329–334. https://doi.org/10.1038/ng843

Maison, C., D. Bailly, D. Roche, R. Montes de Oca, A.V. Probst, I. Vassias, F. Dingli, B. Lombard, D. Loew, J.P. Quivy, and G. Almouzni. 2011. SUMOylation promotes de novo targeting of HP1α to pericentric heterochromatin. *Nat. Genet.* 43:220–227. https://doi.org/10.1038/ng.765

McNulty, S.M., L.L. Sullivan, and B.A. Sullivan. 2017. Human Centromeres Produce Chromosome-Specific and Array-Specific Alpha Satellite Transcripts that Are Complexed with CENP-A and CENP-C. *Dev. Cell.* 42: 226–240.e6. https://doi.org/10.1016/j.devcel.2017.07.001

Miyanari, Y., C. Ziegler-Birling, and M.E. Torres-Padilla. 2013. Live visualization of chromatin dynamics with fluorescent TALEs. *Nat. Struct. Mol. Biol.* 20:1321–1324. https://doi.org/10.1038/nsmb.2680

Musacchio, A., and E.D. Salmon. 2007. The spindle-assembly checkpoint in space and time. *Nat. Rev. Mol. Cell Biol.* 8:379–393. https://doi.org/10.1038/nrm2163

Nagaoka, S.I., T.J. Hassold, and P.A. Hunt. 2012. Human aneuploidy: mechanisms and new insights into an age-old problem. *Nat. Rev. Genet.* 13: 493–504. https://doi.org/10.1038/nrg3245

Ottolini, C.S., L. Newnham, A. Capalbo, S.A. Natesan, H.A. Joshi, D. Cimadomo, D.K. Griffin, K. Sage, M.C. Summers, A.R. Thornhill, et al. 2015. Genome-wide maps of recombination and chromosome segregation in human oocytes and embryos show selection for maternal recombination rates. *Nat. Genet.* 47:727–735. https://doi.org/10.1038/ng.3306

Perea-Resa, C., and M.D. Blower. 2017. Satellite Transcripts Locally Promote Centromere Formation. *Dev. Cell.* 42:201–202. https://doi.org/10.1016/j.devcel.2017.07.017

Perea-Resa, C., and M.D. Blower. 2018. Centromere Biology: Transcription Goes on Stage. *Mol. Cell. Biol.* 38:e00263–18. https://doi.org/10.1128/MCB.00263-18

Pesin, J.A., and T.L. Orr-Weaver. 2008. Regulation of APC/C activators in mitosis and meiosis. *Annu. Rev. Cell Dev. Biol.* 24:475–499. https://doi.org/10.1146/annurev.cellbio.041408.115949

Probst, A.V., I. Okamoto, M. Casanova, F. El Marjou, P. Le Baccon, and G. Almouzni. 2010. A strand-specific burst in transcription of pericentric satellites is required for chromocenter formation and early mouse development. *Dev. Cell.* 19:625–638. https://doi.org/10.1016/j.devcel.2010.09.002

Rošić, S., F. Köhler, and S. Erhardt. 2014. Repetitive centromeric satellite RNA is essential for kinetochore formation and cell division. *J. Cell Biol.* 207: 335–349. https://doi.org/10.1083/jcb.201404097

Santaguida, S., A. Tighe, A.M. D'Alise, S.S. Taylor, and A. Musacchio. 2010. Dissecting the role of MPS1 in chromosome biorientation and the spindle checkpoint through the small molecule inhibitor reversine. *J. Cell Biol.* 190:73–87. https://doi.org/10.1083/jcb.201001036

Seydoux, G., and R.E. Braun. 2006. Pathway to totipotency: lessons from germ cells. *Cell.* 127:891–904. https://doi.org/10.1016/j.cell.2006.11.016

Smurova, K., and P. De Wulf. 2018. Centromere and Pericentromere Transcription: Roles and Regulation … in Sickness and in Health. *Front. Genet.* 9:674. https://doi.org/10.3389/fgene.2018.00674

Susor, A., D. Jansova, R. Cerna, A. Danylevska, M. Anger, T. Toralova, R. Malik, J. Supolikova, M.S. Cook, J.S. Oh, and M. Kubelka. 2015. Temporal and spatial regulation of translation in the mammalian oocyte via the mTOR-eIF4F pathway. *Nat. Commun.* 6:6078. https://doi.org/10.1038/ncomms7078

Swartz, S.Z., L.S. McKay, K.-C. Su, L. Bury, A. Padeganeh, P.S. Maddox, K.A. Knouse, and I.M. Cheeseman. 2019. Quiescent Cells Actively Replenish CENP-A Nucleosomes to Maintain Centromere Identity and Proliferative Potential. *Dev. Cell.* 51:35–48.e7. https://doi.org/10.1016/j.devcel.2019.07.016

Talbert, P.B., and S. Henikoff. 2018. Transcribing Centromeres: Noncoding RNAs and Kinetochore Assembly. *Trends Genet.* 34:587–599. https://doi.org/10.1016/j.tig.2018.05.001

Thanisch, K., K. Schneider, R. Morbitzer, I. Solovei, T. Lahaye, S. Bultmann, and H. Leonhardt. 2014. Targeting and tracing of specific DNA sequences with dTALEs in living cells. *Nucleic Acids Res.* 42:e38. https://doi.org/10.1093/nar/gkt1348

Wong, L.H., K.H. Brettingham-Moore, L. Chan, J.M. Quach, M.A. Anderson, E.L. Northrop, R. Hannan, R. Saffery, M.L. Shaw, E. Williams, and K.H.A. Choo. 2007. Centromere RNA is a key component for the assembly of nucleoproteins at the nucleolus and centromere. *Genome Res.* 17:1146–1160. https://doi.org/10.1101/gr.6022807

Wu, T., S.I.R. Lane, S.L. Morgan, and K.T. Jones. 2018. Spindle tubulin and MTOC asymmetries may explain meiotic drive in oocytes. *Nat. Commun.* 9:2952. https://doi.org/10.1038/s41467-018-05338-7

Zielinska, A.P., E. Bellou, N. Sharma, A.S. Frombach, K.B. Seres, J.R. Gruhn, M. Blayney, H. Eckel, R. Moltrecht, K. Elder, et al. 2019. Meiotic Kinetochores Fragment into Multiple Lobes upon Cohesin Loss in Aging Eggs. *Curr. Biol.* 29:3749–3765.e7. https://doi.org/10.1016/j.cub.2019.09.006

Supplemental material

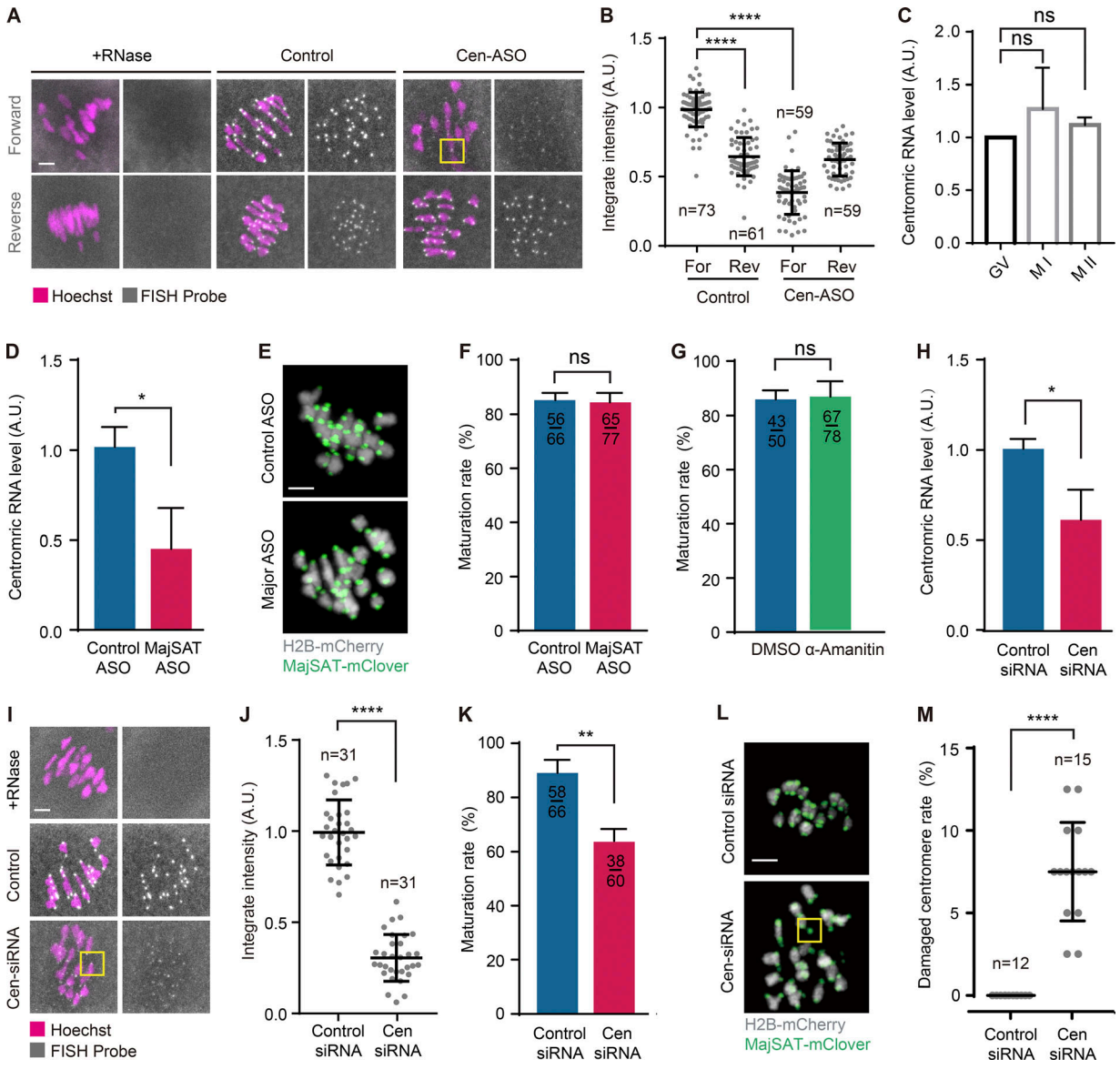

Figure S1. **MinSAT forward transcripts were depleted by RNA interference in MI oocytes. (A)** MinSAT transcripts (forward and reverse) detected with strand-specific RNA FISH probes in MI oocytes (n = 8–12 oocytes combined from three independent experiments for each group). RNase treatment was performed as a negative control. Cen-ASO concentration was 40 µM. Scale bar: 5 µm. **(B)** The intensity of both forward and reverse transcript probes from A was compared with background subtraction. The integrated intensity (fluorescent foci) was measured specifically at the centromeric region (depicted by the yellow box in A). The number of fluorescent foci analyzed is indicated. Data were normalized with respect to the average intensity of forward transcripts (****, $P < 0.0001$, ANOVA with Tukey's post hoc test). **(C)** Levels of MinSAT RNAs in GV, MI, and MII oocytes were tested by qRT-PCR (three independent experiments). Error bars are 95% confidence limits. 30 oocytes are in each group. **(D)** The knockdown efficiency of MajSAT-ASO was tested by qRT-PCR (ASO: 40 µM). All qRT-PCR tests were performed in three independent experiments. P values from 95% CI (*, $P < 0.01$). 30 oocytes in each group. **(E)** The integrity of centromeres shown in live oocytes. **(F)** MI completion rates were compared between control ASO– and MajSAT-ASO–injected oocytes (no significance, χ^2 test). **(G)** MI completion rates were compared between control and α-amanitin (60 µM) treatment (no significance, χ^2 test). **(H)** The knockdown efficiency of Cen-siRNA (40 µM) was tested by qRT-PCR. All qRT-PCR tests were performed in three independent experiments. P value and error bars from 95% CI (*, $P < 0.01$). 30 oocytes in each group. **(I)** Cen-RNA level was tested after siRNA interference by RNA FISH as in A. Scale bar: 5 µm. The fluorescent foci for measurements are indicated (yellow box; n = 6 oocytes combined from two independent experiments). **(J)** The intensity of Cen-RNA levels was measured as in B (****, $P < 0.0001$, t test). **(K)** MI completion rates in control siRNA– and Cen-siRNA–injected oocytes (**, $P < 0.01$, χ^2 test). **(L)** MajSAT signal in an oocyte injected with control siRNA or Cen-siRNA. A damaged centromere is shown by the yellow box. **(M)** The incidence of damaged centromeres in oocytes injected with control siRNA or Cen-siRNA (****, $P < 0.0001$, t test). The average and standard error were calculated based on three independent experiments. Error bars indicate SD.

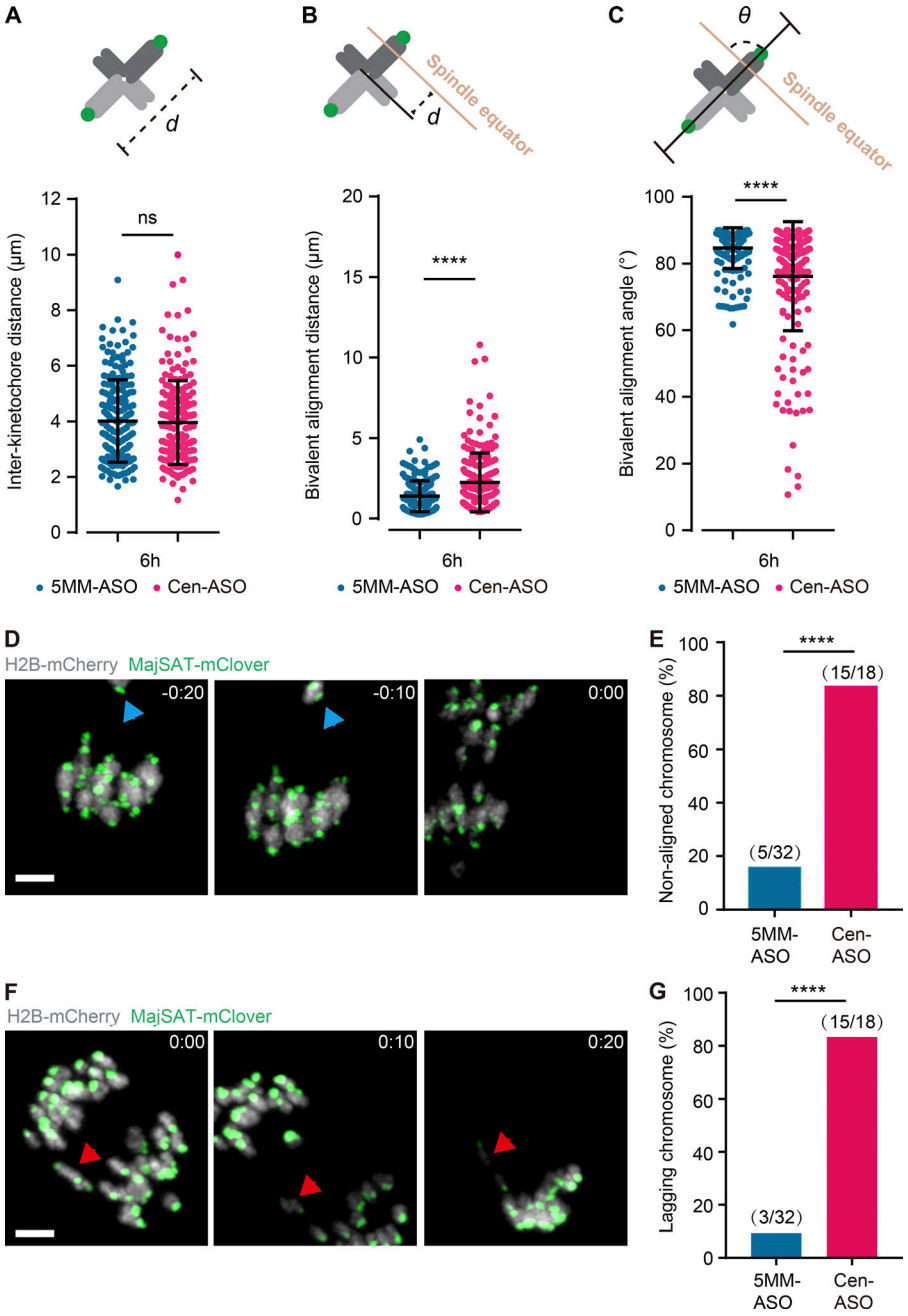

Figure S2. **Cen-RNA depletion induced meiotic defects. (A–C)** Inter-kinetochore distance (A), alignment distance (B), and bivalent angle (C) in bivalents from Cen-ASO– or 5MM-ASO–injected oocytes (200 bivalents from 10 oocytes) at 6 h after NEBD (****, $P < 0.0001$, *t* test). Schematic shows the measurement being made. Error bars indicate SD. **(D)** Representative time-lapse image of a Cen-ASO–injected oocyte expressing H2B-mCherry (gray) and MajSAT-mClover (green). A nonaligned bivalent is labeled by blue arrowheads. Times are relative to anaphase. Scale bar: 5 μm. **(E)** Percentage of oocytes with nonaligned bivalents following injection with either Cen-ASO or 5MM-ASO (****, $P < 0.0001$, χ^2 test). **(F)** Representative time-lapse image of a Cen-ASO–injected oocyte expressing H2B-mCherry (gray) and MajSAT-mClover (green). A lagging chromosome is labeled by the red arrowheads. Times are relative to anaphase. Scale bar: 5 μm. **(G)** Lagging chromosome rates in oocytes injected with either Cen-ASO or 5MM-ASO (****, $P < 0.0001$, χ^2 test). The experiments were performed twice.

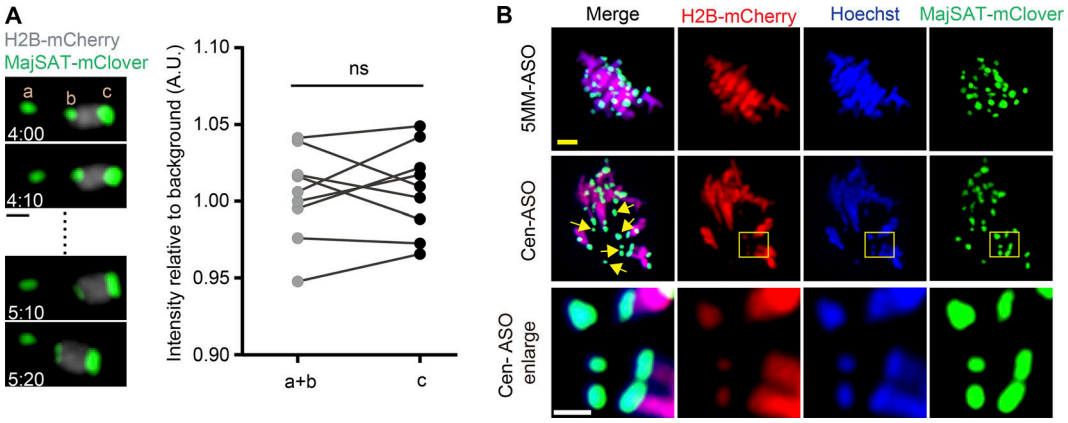

Figure S3. **Representative time-lapse images show the composition of released centromeres. (A)** The total intensity of splitting centromere fragments a and b is equal to intact centromere c (green: MajSAT-mClover; gray: H2B-mCherry). Time from NEBD. Data from nine time points. P value from paired *t* test, P = 0.875. Scale bar: 2 µm. **(B)** The released centromere parts are marked by arrows (blue: Hoechst; green: MajSAT-mClover; red: H2B-mCherry). Scale bar: 5 µm (yellow) and 2 µm (white).

Video 1. **Meiosis I was delayed by Cen-RNA depletion.** Green: MajSAT-mClover; gray: H2B-mCherry. Time from NEBD. Scale bar: 10 µm. Video is played at 6,600× real-time speed.

Video 2. **Visualization the process of centromere breakage.** Green: MajSAT-mClover; gray: H2B-mCherry. Time from NEBD. Scale bar: 2 µm. Video is played at 3,000× real-time speed.